Received: 2 November 2022 | Revised: 4 August 2023 | Accepted: 24 August 2023

DOI: 10.1002/hbm.26480

RESEARCH ARTICLE

WILEY

Microstates of the cortical brain-heart axis

Vincenzo Catrambone | Gaetano Valenza

Neurocardiovascular Intelligence Laboratory, Bioengineering and Robotics Research Center E. Piaggio, & Department of Information Engineering, School of Engineering, University of Pisa, Pisa, Italy

Correspondence
Vincenzo Catrambone, Neurocardiovascular Intelligence Laboratory, Bioengineering and Robotics Research Center E. Piaggio, & Department of Information Engineering, School of Engineering, University of Pisa, Largo L. Lazzarino 1, 56124, Pisa, Italy.
Email: vincenzo.catrambone@ing.unipi.it

Funding information
H2020 Future and Emerging Technologies, Grant/Award Number: 101017727

Abstract

Electroencephalographic (EEG) microstates are brain states with quasi-stable scalp topography. Whether such states extend to the body level, that is, the peripheral autonomic nerves, remains unknown. We hypothesized that microstates extend at the brain-heart axis level as a functional state of the central autonomic network. Thus, we combined the EEG and heartbeat dynamics series to estimate the directional information transfer originating in the cortex targeting the sympathovagal and parasympathetic activity oscillations and vice versa for the afferent functional direction. Data were from two groups of participants: 36 healthy volunteers who were subjected to cognitive workload induced by mental arithmetic, and 26 participants who underwent physical stress induced by a cold pressure test. All participants were healthy at the time of the study. Based on statistical testing and goodness-of-fit evaluations, we demonstrated the existence of microstates of the functional brain-heart axis, with emphasis on the cerebral cortex, since the microstates are derived from EEG. Such nervous-system microstates are spatio-temporal quasi-stable states that exclusively refer to the efferent brain-to-heart direction. We demonstrated brain-heart microstates that could be associated with specific experimental conditions as well as brain-heart microstates that are non-specific to tasks.

KEYWORDS
brain-heart, EEG, HRV, microstates

1 | INTRODUCTION

Wide research supports the idea that brain dynamics measured using electroencephalography (EEG) has transient quasi-stable states that manifest through specific scalp topographies of cerebral activity temporally close to peaks of the global field potential (GFP; Lehmann et al., 1987; Michel & Koenig, 2018; Mishra et al., 2020; Brodbeck et al., 2012; van de Ville et al., 2010; Khanna et al., 2015), which have been defined as brain/EEG *microstates* and associated with *atoms of thought* (Lehmann, 1990; van de Ville et al., 2010). Several prototypical microstates that consistently recur over time have been identified across participants in multiple studies (Brodbeck et al., 2012; Khanna et al., 2015; Lehmann et al., 1987; Michel & Koenig, 2018; Mishra et al., 2020; van de Ville et al., 2010). These microstates are considered the fundamental building blocks of the chain of spontaneous conscious mental processes and have been associated with the level of mentation (Michel & Koenig, 2018). Recent research has shown that the temporal evolution of microstate series varies depending on various physiological processes, such as sleep, motor tasks, mentation, hypnosis, as well as mental and psychiatric disorders (Brodbeck et al., 2012; Katayama et al., 2007; Khanna et al., 2014; Lehmann et al., 2005; Pierpaolo et al., 2022; Pirondini et al., 2017; Tait et al., 2020; Zappasodi et al., 2019). These disorders have been found to manifest EEG microstates with scale-free dynamics (van de Ville et al., 2010).

The occurrence of microstates has been based on the current understanding that brain functions arise from massive parallel processing in diffused and distributed brain networks (Bressler & Menon, 2010; Li et al., 2022). Although microstates have historically been linked to the resting state (RS) of the brain, recent investigations associated microstate dynamics with other functional cognitive activities or physiological conditions (Hu et al., 2022; Katayama et al., 2007; Li et al., 2022; Michel & Koenig, 2018; Pierpaolo et al., 2022; Pirondini et al., 2017). This allowed the identification of numerous cortical and subcortical brain regions whose activity has been linked to microstate dynamics, particularly the insula, thalamus, amygdala, anterior cingulate cortex, and others (Britz et al., 2010; Musso et al., 2010).

Even if not expressively mentioned, these regions reportedly belong to the central autonomic network (CAN; Valenza et al., 2019; Valenza et al., 2020). CAN is not ascribable to a specific brain region, since it encompasses the medullary areas, midbrain and amygdala, thalamus, peripheral autonomic terminations, and cortical regions (e.g., medial prefrontal cortex, anterior cingulate cortex, and insula; Govoni et al., 2020; Valenza et al., 2020). The CAN consists of several components comprising sympathetic and parasympathetic connections to the central nervous system (CNS) and is strictly involved in the definition of functional brain-heart interplay (BHI). Indeed, the BHI represents the functional outcome of a network of chemical, electrical, and anatomical connections that originates in the CAN (Benarroch, 1993; Catrambone & Valenza, 2021; Quadt et al., 2022; Thome et al., 2017; Valenza et al., 2019; Valenza et al., 2020). Research on functional BHI revealed through the analysis of the EEG and heart rate variability (HRV) series revealed that healthy BHI variations occur as physiological responses to several events, such as emotion perception (Candia-Rivera, Catrambone, Thayer, et al., 2022), alternating sleep stages (Silvani et al., 2016), cognitive load (Yu et al., 2018), intentional movements (Catrambone, Averta, et al., 2021), and autonomic maneuvers (Catrambone, Talebi, et al., 2021; Jerath & Barnes, 2009). Moreover, BHI time-series alterations have been reportedly associated with neuropathological conditions, such as mild depression (Catrambone, Messerotti Benvenuti, et al., 2021), epilepsy (Pernice et al., 2022), and schizophrenia (Schulz et al., 2013). Functional BHI is a directional phenomenon, meaning that the influence of brain activity on cardiovascular function is not necessarily equivalent to the influence of heart activity on cerebral dynamics (Catrambone, Messerotti Benvenuti, et al., 2021; Catrambone & Valenza, 2021; Catrambone & Valenza, 2023). Moreover, BHI is a dynamic process that changes over time and in response to physiological conditions. The influence of BHI is diffused across the brain, involving networks such as the CAN, the default mode network, and others.

While previous research has linked EEG microstates to brain regions within the CAN, it is unclear whether microstates also exist at the intersection of the central and autonomic nervous systems (ANS). To explore this possibility, we investigate the functional connections between the brain and heart at rest and under cognitive and physical stress. Our processing pipeline leverages a time-resolved estimation of functional BHI-related GFP, which we refer to as BHI-GFP. By hypothesizing that microstates extend to the brain-heart level, we can explain the global variance of the BHI-GFP series and observe meaningful changes in BHI-microstate dynamics according to experimental elicitation. We tested this hypothesis using two datasets: one that elicited BHI changes through cognitive workload (CW) stress using multiple mental arithmetic (Zyma et al., 2019), and another that employed the cold pressor test (CPT), a well-known method for eliciting a strong sympathovagal response (Catrambone, Talebi, et al., 2021). The purpose of this study is three-fold: (i) to demonstrate the existence of BHI microstates as quasi-stable states in BHI; (ii) to verify the applicability of microstate analysis in the BHI context; and (iii) to examine whether psycho-physiological states affect BHI-derived microstate dynamics.

2 | EXPERIMENTAL RESULTS

The same nervous system-wise analysis framework was applied separately to the two datasets.

2.1 | Cognitive workload task

The experimental results obtained from the analysis of the CW dataset are reported herein. The dataset analysis identified three BHI-microstates for each combination of BHI directions and frequency bands, denoted as $C_{Brain \rightarrow LF}$, $C_{Brain \rightarrow HF}$, $C_{LF \rightarrow Brain}$, and $C_{HF \rightarrow Brain}$, where LF and HF represent HRV-PSD low frequency (LF) and high frequency (HF), respectively. Figure 1 displays the topographies of the identified microstate prototypes, along with their associated global explained variance (GEV). Remarkably, the GEV for both brain-to-heart

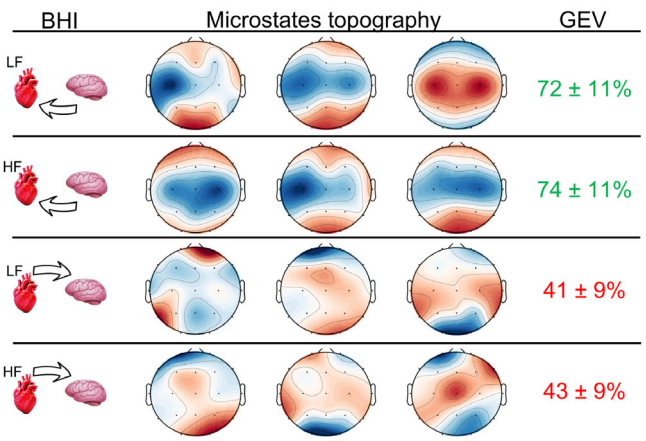

FIGURE 1 Experimental results from the cognitive workload (CW) dataset. The left column makes explicit the direction of the brain-heart interplay (BHI) and heart rate variability (HRV) frequency band involved; the right column reports the global explained variance (GEV), as median across-subject ± standard deviation, associated to the backfitting operation on the microstate prototypes, which are represented in the central part of the figure.

TABLE 1 Number of occurrences for each brain-to-heart BHI microstate (i.e., μ_1,μ_2,μ_3) in the two experimental conditions, normalized per window's time length.

		RS	CW	Total	χ^2	*p*-value
$C_{B\to LF}$	μ_1	39.1	**39.15**	78.25	23.44	$1.7\cdot10^{-9}$
	μ_2	**185.5**	127.55	313.1		
	μ_3	82.67	**135.37**	218.03		
$C_{B\to HF}$	μ_1	44.55	**100**	144.55	33.16	$\approx10^{-15}$
	μ_2	**83.77**	82.72	166.48		
	μ_3	**179**	119.35	298.35		

Note: The results of the statistical analysis performed through χ^2 test for contingency table are reported in the last two columns. Bold numbers indicate the experimental phase during which a specific microstate was more prevalent.

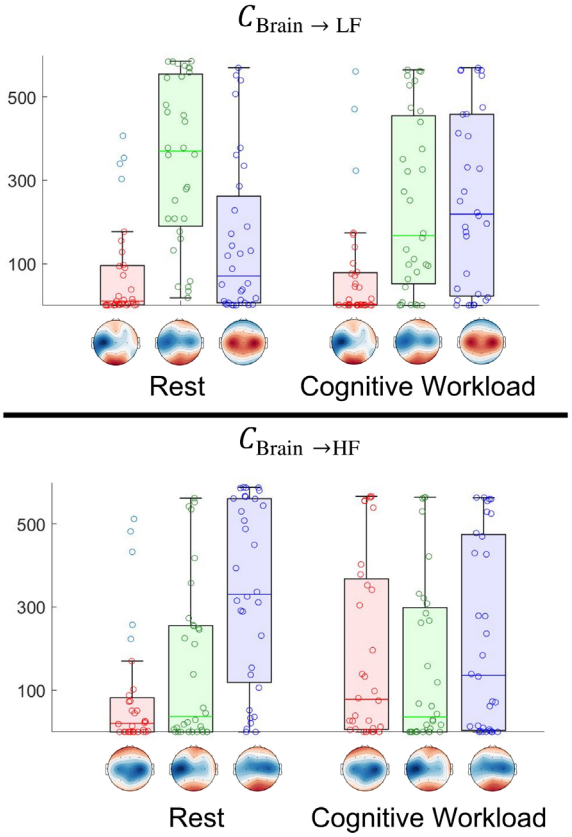

FIGURE 2 Graphical representation of the brain-heart interplay (BHI) microstates occurrences in the two experimental conditions of the CW dataset, for both the heart rate variability (HRV) frequency bands considered (top panel for $C_{\text{Brain}\to\text{LF}}$, and bottom panel for $C_{\text{Brain}\to\text{HF}}$. Each histogram's bar represents the subject-wise sample given by the number of occurrences of given microstates (whose prototype topography is represented at the basis of the histogram bar).

microstates is higher than 70% (approximately 72% for brain-to-LF BHI and 74% for brain-to-HF BHI), indicating that the microstate analysis can effectively explain the spatio-temporal dynamics of $C_{\text{Brain}\to\text{LF}}$ and $C_{\text{Brain}\to\text{HF}}$, while the same is not true in the opposite direction, where the GEV is less than 50% for both $C_{\text{LF}\to\text{Brain}}$ and $C_{\text{HF}\to\text{Brain}}$.

The GEV provides additional information that complements the topographical representation of the prototypes. Indeed, the BHI microstate prototypes extracted from $C_{\text{Brain}\to\text{LF}}$ and $C_{\text{Brain}\to\text{HF}}$ (i.e., both in the direction from the brain to the heart) exhibit a smooth and physiologically plausible distribution, whereas those extracted from $C_{\text{LF}\to\text{Brain}}$ and $C_{\text{HF}\to\text{Brain}}$ have a less continuous and more disrupted distribution. Consequently, due to the limited amount of explained variance and the implausible topographies, we did not consider the heart-to-brain BHI microstates to be robust. As a result, statistical analysis in that direction was not included here, but the results are available in Figure S3 of the Supplementary Material.

Table 1 illustrates the precise number of occurrences of each microstate in the two experimental conditions aggregated for all the participants, and averaged per window length. Figure 2 graphically reports the number of occurrences of each microstate for the different participants under the two experimental conditions. This allows us to verify how the distribution of the three BHI microstates changes from a RS to a CW task. In the context of $C_{\text{Brain}\to\text{LF}}$, the second microstate prototype is the most frequently observed during the RS phase, while it is as frequent as the third microstate during the CW task. In contrast, the first microstate does not appear to undergo a significant change in its frequency of occurrence between the two phases. Turning to $C_{\text{Brain}\to\text{HF}}$ microstates, during the resting state, the occurrences of the three prototypes show a clear inhomogeneity, with the third one being the most frequent and the first one being the least frequent. In contrast, during the CW task, the occurrences of the three microstate prototypes are more evenly distributed. Specifically, the first microstate substantially increases its occurrences (from around 44 to 100), while the third one substantially decreases its occurrence (from 179 to around 119).

To statistically assess the distribution change across the experimental conditions, as explained in Section 4.5, a χ^2 statistical test for contingency table was performed, as reported in Table 1. Moreover, Table 1 reports the statistics performed on both $C_{\text{Brain}\to\text{LF}}$ and $C_{\text{Brain}\to\text{HF}}$ which both show extremely low *p*-values, $\approx10^{-9}$ and 10^{-15} respectively. Interestingly, the same statistical test does not provide any significant difference for non-meaningful microstates, as the heart-to-brain ones (informally defined as non-meaningful since not able to explain the overall dynamics due to a low GEV value), as they distribute randomly and independently from experimental phases (results not presented here, available in Figure S3 of the Supplementary Material).

2.2 | Cold pressor test

The experimental results obtained from the analysis of the CPT dataset identified five BHI microstates across all BHI directions and frequency bands. Figure 3 displays the topographies of the identified microstate prototypes along with their associated GEV. Consistent with the CW dataset, the brain-to-heart BHI microstates have a GEV

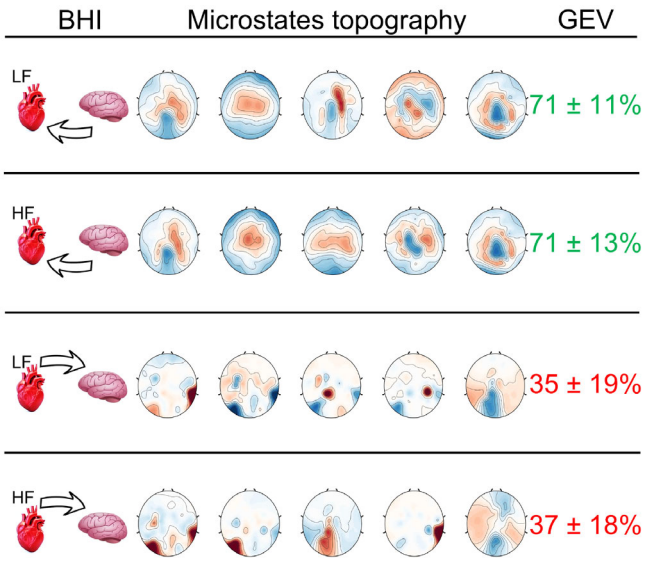

FIGURE 3 Experimental results from the cold pressor test (CPT) dataset. The left column makes explicit the direction of the brain-heart interplay (BHI) and HRV-frequency band involved; the right column reports the global explained variance (GEV), as median across-subject ± standard deviation, associated with the backfitting operation on the microstates prototypes, which are represented in the central part of the figure.

greater than 70%, indicating that the microstate analysis is capable of explaining the spatio-temporal dynamics of $C_{\text{Brain}\to\text{LF}}$ and $C_{\text{Brain}\to\text{HF}}$ (with a GEV of approximately 71% in both HRV bands). In contrast, the GEV in the opposite direction for $C_{\text{LF}\to\text{Brain}}$ (approximately 35%) and $C_{\text{HF}\to\text{Brain}}$ (approximately 37%) is less than 40%. BHI microstate prototypes extracted from $C_{\text{Brain}\to\text{LF}}$ and $C_{\text{Brain}\to\text{HF}}$ in the direction from brain to heart have smoother and more physiologically plausible distributions than those extracted from $C_{\text{LF}\to\text{Brain}}$ and $C_{\text{HF}\to\text{Brain}}$, which appear less continuous and more disturbed. The results shed light on the spatio-temporal dynamics of the BHI and suggest a directionality from the brain to the heart, with more plausible and continuous microstate prototypes. This behavior was also observed in the experimental results for the CW dataset. Due to the limited amount of explained variance and the implausibility of the topographies, statistical analysis on the heart-to-brain BHI microstates are reported in Figure S4 of the Supplementary Material.

The higher number of BHI microstates makes the graphical representation of the results challenging, for which a tabular representation is preferred. Accordingly, these experimental results are reported in Table 2, where the precise number of occurrences of each microstate in the three experimental conditions aggregated for all the participants, and averaged per window length, are reported (per subject statistics of single-microstate occurrences are provided in the Table S1 of the Supplementary material, whereas a graphical representation of Table 2 is provided in Figures S1, S2 of the Supplementary material). In the context of the $C_{\text{Brain}\to\text{LF}}$ direction, the second microstate prototype emerges as the most frequently observed during all phases. Its occurrence reaches its peak during the resting state, gradually decreasing until the lowest occurrence is detected in the recovery phase. Conversely, the first microstate prototype exhibits the lowest occurrence during rest and reaches its peak in the CPT phase. In terms of relative change, the fourth (μ_4) and fifth (μ_5) microstates demonstrate the most substantial variation. The occurrence of μ_5 more than doubles from rest to recovery, while μ_4 reduces its occurrence to one-third during the corresponding phases.

TABLE 2 Number of occurrences for each brain-to-heart brain-heart interplay (BHI) microstate (i.e., $\mu_1,\ldots,\mu_5$) in the three experimental conditions.

		Rest	CPT	Rec	Total	χ^2	*p*-value
$C_{\text{B}\to\text{LF}}$	μ_1	113.5	**126.9**	120.7	361.1	38.1	10^{-18}
	μ_2	**253.6**	247.1	237	737.7		
	μ_3	26.8	28.2	**41.4**	96.4		
	μ_4	**60.5**	37.7	21.2	119.4		
	μ_5	25.6	40.1	**58.5**	124.2		
$C_{\text{B}\to\text{HF}}$	μ_1	50.8	64.8	**95.7**	211.3	61.8	10^{-35}
	μ_2	106.7	105.7	**109.1**	321.5		
	μ_3	239.6	**245.7**	181	666.3		
	μ_4	**62.5**	38.3	34.2	135		
	μ_5	20.4	25.5	**58.7**	104.7		

Note: The results of the statistical analysis performed through χ^2 test for contingency table are also reported in the last two columns. Bold numbers indicate the experimental phase during which a specific microstate was more prevalent.

Shifting to the $C_{\text{Brain}\to\text{HF}}$ direction, the third prototype clearly emerges as the most frequent across all experimental phases, although its occurrence undergoes significant changes among them, decreasing from approximately 240 in rest and CPT to 180 in recovery. Additionally, the presence of the first, fourth, and fifth prototypes (μ_1,μ_4,μ_5, respectively) is strongly influenced by the experimental phases. From initial rest to recovery, μ_1 nearly doubles its occurrence (from 51 to 96, approximately), while μ_4 almost halves its occurrence (from 62 to 34, approximately), and μ_5 triples its occurrence from 20 to 59, approximately.

The BHI-microstate temporal distribution changes from the RS to the CPT phase to recovery, and the statistical analysis provides strong supporting evidences, since the *p*-values obtained are $\approx 10^{-18}$, considering $C_{\text{Brain}\to\text{LF}}$, and $\approx 10^{-35}$ for $C_{\text{Brain}\to\text{HF}}$. It is worth noting that the statistical test performed on dataset CPT did not reveal any significant difference for non-meaningful microstates, such as the heart-to-brain ones. These microstates are informally defined as non-meaningful because of their low GEV value, which implies that they cannot explain the overall dynamics effectively. As a consequence, these microstates distribute randomly and independently from experimental phases. The detailed results of this analysis are available in Figure S4 of the Supplementary Material. Indeed, if the temporal distribution of the BHI-microstates was not affected by the participant's physiological state, which was solicited by the experimental protocol,

then all the microstate occurrence tendencies would not change, and all the microstate occurrences would have an almost uniform distribution across the experimental phase.

2.3 | Microstates comparison between datasets

Figure 4 displays the *p*-values associated with the global dissimilarity (GD) between all pairs of microstates, focusing on the brain-to-LF (left panel) and brain-to-HF interplay (right panel). Notably, concerning the brain-to-LF microstates, all microstates from the first dataset (CW) exhibit significant similarity with at least two prototypes obtained from the CPT dataset. However, two CPT prototypes (i.e., the third and the fifth) show no significant similarity with any of the microstates detected in the CW dataset. Similarly, in the context of brain-to-HF interplay, all CW prototypes identified demonstrate significant similarity with some of the microstates detected in the CPT dataset, with *p*-values reaching as low as $4.1e^{-6}$. However, one CPT microstate lacks any significant global similarity with any of the CW prototypes.

$BHI_{brain\rightarrow LF}$ CW

$BHI_{brain\rightarrow LF}$ CPT \ GD			
	0.02400	**0.00012**	**0.00038**
	0.00033	**$3.5e^{-5}$**	**$5.7e^{-5}$**
	1.00	0.3640	0.45000
	0.65400	**0.018**	**0.000678**
	1.00	0.4340	0.3880

$BHI_{brain\rightarrow HF}$ CW

$BHI_{brain\rightarrow HF}$ CPT \ GD			
	0.0072	0.2580	**0.0073**
	$4.4e^{-5}$	**0.00053**	**$7.3e^{-5}$**
	$2.4e^{-5}$	**$5.3e^{-5}$**	**$4.1e^{-6}$**
	0.624	0.632	**0.016**
	0.5978	0.631	0.7720

FIGURE 4 *p*-values associated to global dissimilarity (GD) calculated for all BHI brain-to-LF (left panel) and brain-to-HF (right panel) microstates, extracted during resting state in CPT dataset (rows) and CW dataset (columns). Colored cells and bold text highlight significant GD (*p*-value < .05).

3 | DISCUSSION AND CONCLUSION

The main objective of this study was to investigate the possibility of detecting quasi-stable states in the dynamics of the cortical brain-heart axis using the microstate technique. Specifically, we aimed to explore the extent to which the microstates approach can be used to identify and analyze the spatio-temporal patterns of the functional brain-heart interactions. Since the brain regions associated with cortical EEG microstates belong to the CAN (Britz et al., 2010; Musso et al., 2010), we hypothesized that the brain-heart microstates, identified at the cortical level using EEG and heartbeat dynamic analysis, could exist as well. Functional BHI comprises dynamic time-resolved measurements that could be quasi-stable in topography based on the standard microstate definition. Thus, we engineered an analysis pipeline that builds a BHI-associated GFP starting from an electrode-wise BHI directional time-resolved estimation through the synthetic data generation (SDG) model (Catrambone et al., 2019), and then exploited the EEG-microstate analysis to identify the microstate prototypes fitted with the participant experimental series. We performed statistical analysis to test the obtained BHI-microstate goodness of fit, and test whether microstate occurrences change across different experimental phases. The present study used two available experimental datasets already used in BHI studies: the first concurrently elicited the CNS and the ANS responses through CW, and the second was characterized by a strong sympathovagal stimulation delivered via a CPT. Specific discussion is presented as follows.

3.1 | Directional asymmetry

Experimental results demonstrated a clear asymmetry between the brain-to-heart and heart-to-brain directional BHI systems. Indeed, analyses of both the datasets in the top-down direction (i.e., brain-to-heart) resulted in the definition of the microstate prototypes that were physiologically plausible and well-fitted BHI dynamics in terms of the GEV, considering both the HRV frequency bands. Conversely, the microstate analysis performed in the bottom-up direction (i.e., from the heart to the brain) did not effectively summarize the electrode-wise BHI behavior, even when considering both the HRV LF and HF bands. As a result, it was not possible to identify meaningful microstates that could capture the complex spatio-temporal patterns of the BHI in this direction.

The consistency of this result obtained by multiple datasets and frequency bands allows, with some limitations, a high-level consideration about directionality. Indeed, BHI is known to be a strongly directional phenomenon, and brain-to-heart interplay significantly differs from the heart-to-brain one (Govoni et al., 2020); nevertheless, this study suggests that BHI microstates exist, but only in the direction from the brain to the heart. The authors believe that this discrepancy is intrinsic to the BHI phenomenon and entwined to the capability of the microstate analysis. As mentioned previously, BHI in the form of CNS control over ANS activity takes place at different levels and involves multiple brain networks (e.g., CAN and default mode

network) whose activity reverberates throughout and concurrently takes input from the entire scalp (Valenza et al., 2019, 2020). In contrast, direct cortical CNS responses to electrophysiological heart activity occur in different brain regions separately at the electrode level (e.g., see heartbeat evoked potentials; Coll et al., 2021), which could be a more spatially and temporally localized process (Pollatos et al., 2005) rather than a whole-brain one manifesting quasi-stable states. Furthermore, microstate analysis builds upon the hypothesis that quasi-stable states exist across the spatio-temporal scalp activity distribution and thereby, could be a powerful tool for capturing diffuse whole-brain behavior and might not capture transient localized brain activity (van de Ville et al., 2010). Thus, to summarize, the main reasons supporting the existence of BHI-microstates only in the brain-to-heart direction rely on this analysis capability to capture diffuse whole-brain behavior, and on the intrinsic BHI features being more diffuse over the scalp in the descending direction. Speculating these results from the viewpoint of the *global workspace model* (Dehaene et al., 1998) might attribute the brain-to-heart interplay to the *unique global workspace* and the heart-to-brain interplay to *specialized and modular processors* (Dehaene et al., 1998), without necessarily labeling them as conscious processes.

3.2 | Task-specific microstates

The experimental results reported in this study translate to the BHI domain what was already known about EEG-microstates being task-specific. Although most of the literature investigating EEG microstates mainly focused on the resting state, most studies often employ the same handful of microstate prototypes, studies based on diverse experimental protocols proved that different conditions lead to task-specific EEG-microstate definitions (Michel & Koenig, 2018; van de Ville et al., 2010). Our analysis revealed the presence of three distinct microstates in the CW task dataset (consisting of a RS and a mental arithmetic task) and five microstates in the CPT dataset (which was divided into rest, CPT, and recovery phases, each lasting 3 min) for both brain-to-LF and brain-to-HF directions. The greater number of microstates identified in the CPT dataset compared to the CW dataset may be attributed to the higher complexity of the cognitive task required by the CPT protocol. In fact, while the CW tasks elicit cognitive and affective stress (Zyma et al., 2019), the CPT also involves pain and haptic perception, together with motor control and a strong sympathovagal response (Catrambone, Barbieri, et al., 2021; Chang et al., 2002). It is possible that the increased cognitive demands of the CPT task resulted in more pronounced changes in the spatio-temporal dynamics of the BHI, which were captured by the microstate analysis.

However, we conducted a comprehensive statistical comparison between the microstate prototypes' topographies extracted from the two datasets at a spatial level. The results highlighted the consistency between the identified microstates and the physiological processes underlying the BHI phenomenon. Nonetheless, we acknowledge the presence of some differences in the microstate configurations related to BHI. We believe these discrepancies can be attributed to two main factors. First, inherent variations may arise due to the relatively small sample sizes in the datasets, with 32 and 26 subjects for CW and CPT, respectively. Conducting further analyses on larger cohorts would be valuable in establishing a more universal BHI microstate configuration, especially during the resting state. Second, it is crucial to note that the datasets, particularly the EEG data, underwent different preprocessing procedures. Unfortunately, due to the use of different experimental equipment in the two experiments, specifically the preprocessed nature of the CW dataset that had already been published, it was not feasible to replicate the specific preprocessing pipeline in a homogeneous manner. Despite these challenges, our study provides valuable insights into the BHI phenomenon and the microstate configurations related to it. Future research endeavors, focusing on larger sample sizes and standardizing data acquisition and preprocessing methods, would be instrumental in furthering our understanding of the neural mechanisms underlying BHI.

3.3 | Spatio-temporal changes

Considering the dynamic changes and evolution of the BHI microstate occurrences, it was found that both CW and CPT elicitation results in statistically significant changes in the distribution of occurrences of the previously identified microstates.

Regarding the CW task, the microstate analysis for both brain-to-LF and brain-to-HF dimensions revealed the presence of a "resting state" microstate prototype, which occupies most of the resting phase and decreases its relative occurrence during the mental task. This prototype was identified as a microstate μ_2 in the brain-to-LF dimension and a microstate μ_3 in the brain-to-HF dimension. In addition to this prototype, two other microstates were found to have a relative presence change between the RS and the task phase.

Similar considerations were made for the CPT results, where brain-to-LF and brain-to-HF analyses identified five microstate prototypes. Table 2 shows that the second prototype (μ_2) is the most frequent during the RS in the brain-to-LF analysis, while the third prototype (μ_3) is the most frequent in the brain-to-HF analysis during the same phase. Figure 3 shows the topographical representation of these prototypes, which are extremely similar among themselves and share this similarity with the most frequent microstate identified in the analysis of the CW task. Specifically, the topography can be described as a gradient map extending from the central area of the scalp to the most external regions, particularly along the vertical axis. These prototypes have the same gradient going from the central region to the peripheral regions, which is also present in similar topography but with inverted polarity (e.g., μ_3 of the $C_{\text{Brain}\rightarrow\text{LF}}$ microstates extracted in the CW dataset). At the speculation level, it is possible to infer that these topographies might represent non-specific microstates associated with the brain-to-heart interplay during rest. Additionally, at a speculation level, owing to the timing in the order of seconds and its whole-brain nature, we may associate calcium waves in the brain as involved in the directional, descending brain-heart communication.

3.4 | Study limitations and further developments

Although informative, the two experimental paradigms cannot be considered exhaustive, and further investigations are needed to confute such considerations about BHI-microstate directionality, together with other factors directly influencing BHI, such as respiration (Zaccaro et al., 2022). We acknowledge that BHI microstates may extend to subcortical regions, and we recognize the importance of investigating both cortical and subcortical microstates of the brain-heart axis. However, in this study, we focus solely on the microstates of the cortical brain-heart axis. Future work could explore subcortical microstates of the BHI by utilizing brain data, including functional magnetic resonance imaging and cardiovascular variability series. From a methodological viewpoint, we exploited an ad-hoc model based on SDG that can provide time-resolved channel-wise estimation of directional functional BHI (Catrambone et al., 2019) and has been validated in several pathophysiological conditions (Candia-Rivera, Catrambone, Barbieri, & Valenza, 2022; Catrambone & Valenza, 2021). Nevertheless, functional BHI assessments may be performed using different methods at a single EEG channel level. For example, some methods focused on the direct fast brain response to a single heartbeat, namely heartbeat evoked potentials (for a review see; Park & Blanke, 2019), while others have attempted to estimate the information exchange in a larger time window (Catrambone & Valenza, 2021; Faes et al., 2011; Pernice et al., 2022). Moreover, it has been argued that the spectral approach to quantify ANS activity through LF and HF separation is not specific for sympathetic or vagal activity only; nevertheless, its use remains a public standard in the scientific community (Rajendra Acharya et al., 2006; Valenza et al., 2018). Future developments about BHI-microstates may be directed toward a source localization analysis to better characterize the physiological meaning of the microstates.

3.5 | Conclusion

We demonstrated the existence of microstates of the brain-heart axis, focusing on cortical dynamics as estimated through EEG series and heartbeat dynamics from ECG. Such nervous-system-wise microstates are spatio-temporal quasi-stable states that refer exclusively to the efferent brain-to-heart direction and changes in the number and topography under different experimental conditions. Most brain-heart microstates are non-specific to tasks, including physical or mental stress. We may also conclude that directional, descending brain-heart communication not only originates at a single region level but also functionally at the whole-brain level. Overall, the study provides insights into the complex and dynamic nature of the BHI and highlights the potential of microstate analysis as a useful tool for studying brain-heart interactions. The extension of EEG microstates to the body level might open novel perspectives in the study of interoception and might be considered as "*atoms of interoception*".

4 | MATERIALS AND METHODS

4.1 | Experimental data and preprocessing

Two separate experimental paradigms eliciting concurrent CNS and ANS responses were used to validate the proposed system-wise BHI analytical framework. This study was formally approved by the local ethics committee of the University of Pisa under protocol number 0036590/2021.

4.1.1 | Cognitive workload dataset

One of the numerous noninvasive ways to activate the ANS through CNS manipulation is to allow human participants to perform CW through mental arithmetic. A generic paradigm consists of asking participants to complete cognitive tasks repetitively by clicking a button or performing mental algebraic calculations in a controlled time window (Zygmunt & Stanczyk, 2010). In addition to the obvious cognitive functionality involving high-level brain regions, these tasks strongly stress the ANS; in fact, CW tasks have been investigated at both the CNS (Inouye et al., 1993; Wang & Sourina, 2013) and ANS (Bernardi et al., 2000) levels separately; however, only a few studies have focused on their functional BHI correlates (Catrambone & Valenza, 2023). It has been found that in response to stress, modulation of the cardiovascular activity is related to cerebral activity in the left frontal and temporal areas (Gray et al., 2007). Furthermore, studies have shown that during the CW task, there is an increased flow of information originating from the posterior-central and central lobes of the brain directed toward the heart (Yuan et al., 2010). Thus, the first dataset (CW) analyzed was *EEG during mental arithmetic tasks* (Zyma et al., 2019), published in the Physionet.org data repository (https://physionet.org/content/eegmat/1.0.0/).

This dataset consists of concurrent recordings of electrophysiological brain (EEG), using a 10–20 standard 19 electrodes cap, and a 1-lead cardiovascular (ECG) activity, sampled at 500 H, from 36 healthy participants who volunteered to perform 3 min of CW following an equally long initial resting state. Signals from four participants were rejected owing to gross artifacts after visual inspection. Eventually, data from 32 participants (8 males, 18 ± 2.01 years on average) were used for further analysis. The eligibility criteria for the study included subjects with normal or corrected-to-normal vision, normal color perception, no clinical history of mental or cognitive impairment, and no learning disabilities. Specific exclusion criteria included psychiatric or neurological complaints, drug or alcohol addiction, and the use of psychoactive medication.

Data were provided after preprocessing, performed through a power line notch at 50 Hz, followed by $[0.5 - 45]$ Hz band-pass filtering, and independent component analysis was used to reject common artifacts (i.e., ocular, muscular, and cardiac). More details on this dataset, including acquisition and signal preprocessing, are available in (Zyma et al., 2019).

4.1.2 | Cold pressor test dataset

CPT is a commonly used autonomic maneuver aimed at verifying the body's autonomic functionality and CNS response to rapid and maintained temperature stimuli delivered by contact (Cui et al., 2002; Ferracuti et al., 1994; Lovallo, 1975), commonly submerging a distal limb (i.e., hand or foot) or face, in cold water, with a temperature maintained between 0 and 4°C for 1–5 min. Indeed, CPT strongly activates the body systems, such as the baroreflex and the sympathetic nervous system, to actively respond to the allostatic state induced by the stimulation to return to the homeostatic equilibrium (Cui et al., 2002). On the EEG side, cortical and subcortical brain regions elicited by the CPT have been detected in the frontal areas in a wide spectrum, bilateral temporal parts in the β frequency band, and posterior-parietal regions in the α band (Catrambone, Talebi, et al., 2021; Chang et al., 2002; Ferracuti et al., 1994). Previous studies have addressed CPT-induced BHI changes (Candia-Rivera, Catrambone, Barbieri, & Valenza, 2022; Catrambone, Barbieri, et al., 2021; Catrambone & Valenza, 2023), finding diffuse bidirectional interplay, with a preferred directed intervention from brain dynamics to heartbeat (Candia-Rivera, Catrambone, Barbieri, & Valenza, 2022; Catrambone et al., 2019; Catrambone, Talebi, et al., 2021). Thus, an organ-level whole-brain approach for BHI estimation should be particularly suitable for this experimental environment.

The second dataset (CPT) employed was recorded from 24 healthy volunteers (26.7 years on average; 9 females), all right-handed. The participants were seated on a comfortable chair; cold pressor stimulation was performed after an initial 3 min resting state. The CPT was implemented by asking the participants to hold the non-dominant hand (i.e., the left hand) into a basket full of iced water for up to 3 min, a time threshold that researches attests as not eliciting pain perception on average (Cui et al., 2002). However, the volunteers were not constricted and completely free to remove their hands if they felt uncomfortable.

Electrophysiological recordings were obtained employing a 128-electrodes EEG and 1-lead ECG with a sampling frequency of 500 Hz. No subject, recording devices, or any instrumentation was in common between the two datasets (i.e., CW and CPT).

The ECG raw series were bandpass filtered and analyzed using the Pan–Tompkins algorithm (Pan & Tompkins, 1985) to detect R-peaks, which were subsequently analyzed using the Kubios Software (Tarvainen et al., 2014) to reject artifacts, and finally visually inspected for further analysis. EEG series preprocessing was performed partially following the Harvard Automated Processing Pipeline (HAPPE), proposed and described in detail in (Gabard-Durnam et al., 2018), using the MATLAB (MathWorks Inc.) EEGLAB toolbox (Delorme & Makeig, 2004). Briefly, the peripheral channels were rejected, followed by bandpass series (between 1 and 100 Hz) and notch (at 50 Hz) filtering. We identified and removed artifacted channels by calculating the area under the curve for each channel and marking it as artifacted if it exceeded 3 standard deviations of the distribution of all channels. The remaining channels were compared with their neighbors using the weighted-by-distance-correlation as a distance metric. To improve the accuracy of microstate results, we re-referenced the channels offline using the REST method (Yao, 2001), which has been recommended in previous microstate investigations (Hu et al., 2018). The REST method involves transforming EEG data into a reference-independent source space and then back-projecting the data onto the scalp electrodes using a weighting matrix. This method has been shown to enhance the reliability and reproducibility of EEG microstate analysis.

4.2 | Signal preprocessing

The time-resolved power spectral density (PSD) on the EEG time series was obtained by the well-known short-time Fourier transform using a Hamming window of 2 s (that is, 1000 samples) and a window step of 0.1 s, resulting in time series sampled at 10 Hz. The PSD was then integrated into the commonly analyzed EEG spectral band between 1 and 45 Hz. On the other hand, the time-resolved PSD on the HRV series was estimated using the smoothed pseudo-Wigner-Ville distribution integrated into the interval 0.04 Hz–0.15 Hz (i.e., power in the low-frequency band LF) as a non-specific marker of sympathovagal activity, and in the range 0.15 Hz–0.4 Hz (i.e., power of high-frequency HF band) for parasympathetic activity. The two PSD power series derived from HRV (LF and HF) were sampled at 10 Hz to be homogeneous with those derived from the EEG.

4.3 | Brain-heart interplay estimation

BHI reports were produced using a SDG model (Catrambone et al., 2019). Formally, the model constructs an EEG series according to a multi-oscillator model whose amplitudes are generated by a first-order exogenous autoregressive process (Al-Nashash et al., 2004), where the exogenous term models time-resolved communication from the heart to the brain.

Meanwhile, the RR dynamics were modeled by extending the pulse frequency modulation model proposed by Brennan et al. (2002), where the function driving sympathovagal activity has an exogenous term, representing the direction-specific from brain-to-heart coupling index.

In summary, time-varying directional BHI biomarkers represent an immediate assessment of heart-to-brain and brain-to-heart interactions for combinations of EEG and HRV frequency components, respectively. The main idea behind the conceptualization of this model is that the electrophysiological signals of the two systems are not independent from each other, and the introduced coupling terms attempt to formalize these interactions. More specifically, a positive value of $C_{B\rightarrow HF}(t_n)$ indicates that at time t_n, an increase in the EEG-PSD in frequency band B is associated with a proportional increase in the HRV-PSD series in the HF band. In other words, the power of the EEG signal in the specified frequency band is positively correlated with the power of the HRV signal in the HF band, suggesting a functional relationship between the two signals.

The inverse model formulation and derivation of the entire BHI biomarker suite are extensively described in (Catrambone et al., 2019; Catrambone, Messerotti Benvenuti, et al., 2021), and an easy-to-use MATLAB implementation is freely available in (https://it.mathworks.com/matlabcentral/fileexchange/72704-brain-heart-interaction-indexes). To calculate the directional BHI indices, we used the framework described above, which involved separate analysis of the HRV-PSD in the LF and HF bands, as well as the EEG-PSD spectrum in the $[1-45]$ Hz range. Specifically, we extracted the following directional BHI indices: $C_{\text{Brain}\to\text{LF}}$, $C_{\text{Brain}\to\text{HF}}$, $C_{\text{LF}\to\text{Brain}}$, and $C_{\text{HF}\to\text{Brain}}$. These indices reflect the directional influence between the brain and heart, with $C_{\text{Brain}\to\text{LF}}$ and $C_{\text{Brain}\to\text{HF}}$ indicating the influence of brain dynamics on the HRV-PSD in the LF and HF bands, respectively, and $C_{\text{LF}\to\text{Brain}}$ and $C_{\text{HF}\to\text{Brain}}$ indicating the influence of the HRV-PSD in the LF and HF bands on the EEG-PSD.

4.4 | BHI-microstates derivation

The procedure to identify and extract microstates from normal EEG activity is standard and can be found in a comprehensive description in (Michel & Koenig, 2018) and a freely available MATLAB toolbox (Poulsen et al., 2018). In this study, the procedure was adapted for the estimation of BHI microstates.

To derive BHI microstates, we first substituted the EEG series with the BHI series to calculate the topographic maps of BHI-derived GFP. Here, BHI-GFP corresponds to the spatial standard deviation of BHI, estimating the time-resolved amount of BHI accounting for the data of all EEG electrodes, following the definition of EEG-GFP (Skrandies, 1990).

Next, BHI-GFP peaks were identified, and a modified k-means algorithm was used to cluster the BHI-GFP instants to the spatial prototypes. The number of BHI-microstates was chosen based on a meta-criterion that considers a trade-off between different measures of fit (GEV, cross-validation criterion, Krzanowski–Lai criterion, and dispersion; Michel & Koenig, 2018) and the physiological plausibility of topographical maps individuated by the algorithm.

After selecting the microstate prototypes, they were fitted to the entire BHI series. During this procedure, each BHI topographical sample was assigned to a specific microstate prototype based on the level of similarity. The goodness of fit was measured using the GEV, which quantifies the amount of variance of the original GFP dynamics explained by the newly obtained microstate occurrence time series. To ensure continuity, a smoothing operation was implemented using a smoothing window of 250 ms with no overlap, as sharp changes in the obtained series could be attributed to physiological and algorithmic noise (Poulsen et al., 2018).

Due to dataset peculiarity (e.g., number of channels, preprocessing procedure, and task), the BHI-microstates derivation was performed separately for dataset CW and CPT. Different BHI spatiotemporal dynamics elicited by different experimental datasets (i.e., CW and CPT in this study) are expected to result in different numbers and configurations of microstates, similar to classical EEG microstate analysis (Michel & Koenig, 2018). Furthermore, the BHI-microstates derivation was performed once for all the experimental phases enclosed in the same dataset, meaning that, for example, the same microstates were derived from both resting state, cold pressor phase, and recovery phase of the CPT dataset. This was done following the hypothesis that if no spatiotemporal changes were present, then the same microstates would occur with a similar frequency of occurrences. A statistical analysis was conducted to verify this hypothesis. The microstates derivation analysis was repeated independently for all combination of BHI directions (i.e., brain-to-heart and heart-to-brain) and HRV frequency bands (i.e., LF and HF).

4.5 | Statistical analysis

The primary objective of this study was threefold. First, we aimed to verify the existence of BHI microstates. Second, we sought to evaluate the ability of the microstate technique to explain the dynamics of the BHI. Lastly, we aimed to investigate whether the BHI dynamics change in response to sympathovagal elicitation.

To assess the existence of BHI microstates and the capability of the technique to capture their dynamics, we utilized the GEV of the channel-wise BHI time series. This measure provided an estimate of the microstate's ability to explain the global variance of the estimated BHI across the scalp. Additionally, we qualitatively evaluated the physiological plausibility of the extracted microstate topographies, as is commonly performed during EEG artifact rejection procedures. These operations were implemented separately considering different HRV-related frequency bands and BHI directions.

Second, under the null hypothesis of no variation during different stimuli, the number of occurrences of each microstate should not change. To verify this, we exploited the χ^2 statistical test for the contingency table.

A schematic representation of the processing pipeline is shown in Figure 5.

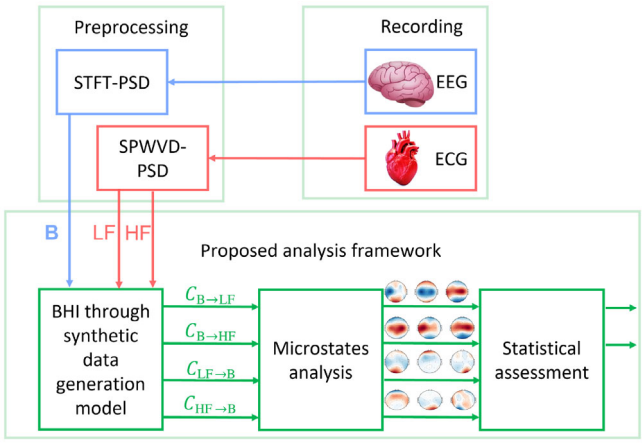

FIGURE 5 Schematic representation of the proposed computational methodology.

4.6 | Quantitative comparison between microstates

To quantitatively assess the comparison of microstate topographies, we employed the GD, a widely-used measure in EEG microstate studies (Murray et al., 2008; Pierpaolo et al., 2022; Zappasodi et al., 2017). It is important to note that microstate prototypes are polarity invariant, meaning that both topographic homogeneity and topographic inversion are considered equivalent. Consequently, the GD is a non-linear measure, assuming minimal and maximal values for equivalent topographies. To ensure comparability between the prototypes from the two datasets, we applied an interpolation procedure to the microstate prototypes obtained in the CW analysis, resulting in prototypes with the same number of channels as those obtained using CPT. Our analysis focused on the brain-to-LF and brain-to-HF frequency bands based on previous results.

To assess the statistical robustness of the measured GD, we performed 1000 random permutations for each comparison, creating a null distribution of surrogate data composed of randomly independent topographies. Each permutation involved shuffling the values across different channels of the prototypes being compared (e.g., microstate 1 of the CPT dataset and prototype 1 of the CW dataset), thereby preserving the same statistical characteristics as the original data. By comparing the real GD value with the permuted ones, we obtained a *p*-value, enabling us to make statistically informed conclusions about the dissimilarity or similarity of microstate topographies between the two datasets.

FUNDING INFORMATION

The research leading to these results has received partial funding from the European Commission H2020 Framework Programme under Grant No. 101017727 of the project EXPERIENCE, and the Italian Ministry of Education and Research (MIUR) in the framework of the FoReLab ad CrossLab projects (Departments of Excellence).

CONFLICT OF INTEREST STATEMENT

All authors declare that they have no conflicts of interest.

DATA AVAILABILITY STATEMENT

Experimental data and software tools are made publicly available. More specifically: the first dataset, that is, *EEG during mental arithmetic tasks* (Zyma et al., 2019), is published in the Physionet.org data repository (https://physionet.org/content/eegmat/1.0.0/); the second dataset, if ethical requirements are met, will be provided to interested researchers via reasonable mail requests. SDG model for BHI estimation has an easy-to-use MATLAB implementation freely available at (https://it.mathworks.com/matlabcentral/fileexchange/72704-brain-heart-interaction-indexes), and microstate analysis toolbox is available at (Poulsen et al., 2018).

ORCID

Vincenzo Catrambone https://orcid.org/0000-0001-9030-7601
Gaetano Valenza https://orcid.org/0000-0001-6574-1879

REFERENCES

Al-Nashash, H., Al-Assaf, Y., Paul, J., & Thakor, N. (2004). EEG signal modeling using adaptive Markov process amplitude. *IEEE Transactions on Biomedical Engineering*, *51*(5), 744–9751.

Benarroch, E. E. (1993). The central autonomic network: Functional organization, dysfunction, and perspective. *Mayo Clinic Proceedings*, *68–10*, 988–1001.

Bernardi, L., Wdowczyk-Szulc, J., Valenti, C., Castoldi, S., Passino, C., Spadacini, G., & Sleight, P. (2000). Effects of controlled breathing, mental activity and mental stress with or without verbalization on heart rate variability. *Journal of the American College of Cardiology*, *35*(6), 1462–1469.

Brennan, M., Palaniswami, M., & Kamen, P. (2002). Poincare plot interpretation using a physiological model of HRV based on a network of oscillators. *American Journal of Physiology-Heart and Circulatory Physiology*, *283*(5), H1873–H1886.

Bressler, S. L., & Menon, V. (2010). Large-scale brain networks in cognition: Emerging methods and principles. *Trends in Cognitive Sciences*, *14*(6), 277–290.

Britz, J., van de Ville, D., & Michel, C. M. (2010). Bold correlates of EEG topography reveal rapid resting-state network dynamics. *NeuroImage*, *52*(4), 1162–1170.

Brodbeck, V., Kuhn, A., von Wegner, F., Morzelewski, A., Tagliazucchi, E., Borisov, S., Michel, C. M., & Laufs, H. (2012). EEG microstates of wakefulness and NREM sleep. *NeuroImage*, *62*(3), 2129–2139.

Candia-Rivera, D., Catrambone, V., Barbieri, R., & Valenza, G. (2022). Functional assessment of bidirectional cortical and peripheral neural control on heartbeat dynamics: A brain-heart study on thermal stress. *NeuroImage*, *251*, 119023.

Candia-Rivera, D., Catrambone, V., Thayer, J. F., Gentili, C., & Valenza, G. (2022). Cardiac sympathetic-vagal activity initiates a functional brain-body response to emotional arousal. *Proceeding of the National Academy of Science*, *119*(21), e2119599119.

Catrambone, V., Averta, G., Bianchi, M., & Valenza, G. (2021). Toward brain–heart computer interfaces: A study on the classification of upper limb movements using multisystem directional estimates. *Journal of Neural Engineering*, *18*(4), 046002.

Catrambone, V., Barbieri, R., Wendt, H., Abry, P., & Valenza, G. (2021). Functional brain–heart interplay extends to the multifractal domain. *Philosophical Transactions of the Royal Society A*, *379*(2212), 20200260.

Catrambone, V., Greco, A., Vanello, N., Scilingo, E. P., & Valenza, G. (2019). Time-resolved directional brain–heart interplay measurement through synthetic data generation models. *Annals of Biomedical Engineering*, *47*(6), 1479–1489.

Catrambone, V., Messerotti Benvenuti, S., Gentili, C., & Valenza, G. (2021). Intensification of functional neural control on heartbeat dynamics in subclinical depression. *Translational Psychiatry*, *11*(1), 1–10.

Catrambone, V., Talebi, A., Barbieri, R., & Valenza, G. (2021). Time-resolved brain-to-heart probabilistic information transfer estimation using inhomogeneous point-process models. *IEEE Transactions on Biomedical Engineering*, *68*(11), 3366–3374.

Catrambone, V., & Valenza, G. (2021). *Functional brain-heart interplay: From physiology to advanced methodology of signal processing and modeling*. Springer Nature.

Catrambone, V., & Valenza, G. (2023). Nervous–system–wise functional estimation of directed brain–heart interplay through microstate occurrences. *IEEE Transactions on Biomedical Engineering*, *70*, 2270–2278.

Chang, P. F., Arendt-Nielsen, L., & Chen, A. C. (2002). Dynamic changes and spatial correlation of eeg activities during cold pressor test in man. *Brain Research Bulletin*, *57*(5), 667–675.

Coll, M.-P., Hobson, H., Bird, G., & Murphy, J. (2021). Systematic review and meta-analysis of the relationship between the heartbeat-evoked potential and interoception. *Neuroscience & Biobehavioral Reviews*, *122*, 190–200.

Cui, J., Wilson, T. E., & Crandall, C. G. (2002). Baroreflex modulation of muscle sympathetic nerve activity during cold pressor test in humans. *American Journal of Physiology-Heart and Circulatory Physiology*, *282*(5), H1717–H1723.

Dehaene, S., Kerszberg, M., & Changeux, J.-P. (1998). A neuronal model of a global workspace in effortful cognitive tasks. *Proceedings of the National Academy of Sciences*, *95*(24), 14529–14534.

Delorme, A., & Makeig, S. (2004). EEGlab: An open source toolbox for analysis of single-trial EEG dynamics including independent component analysis. *Journal of Neuroscience Methods*, *134*(1), 9–21.

Faes, L., Nollo, G., & Porta, A. (2011). Information-based detection of nonlinear granger causality in multivariate processes via a nonuniform embedding technique. *Physical Review E*, *83*(5), 051112.

Ferracuti, S., Seri, S., Mattia, D., & Cruccu, G. (1994). Quantitative EEG modifications during the cold water pressor test: Hemispheric and hand differences. *International Journal of Psychophysiology*, *17*(3), 261–268.

Gabard-Durnam, L. J., Mendez Leal, A. S., Wilkinson, C. L., & Levin, A. R. (2018). The Harvard automated processing pipeline for electroencephalography (happe): Standardized processing software for developmental and high-artifact data. *Frontiers in Neuroscience*, *12*, 97.

Govoni, S., Politi, P., & Vanoli, E. (2020). *Brain and heart dynamics*. Springer.

Gray, M. A., Taggart, P., Sutton, P. M., Groves, D., Holdright, D. R., Bradbury, D., Brull, D., & Critchley, H. D. (2007). A cortical potential reflecting cardiac function. *Proceedings of the National Academy of Sciences*, *104*(16), 6818–6823.

Hu, S., Karahan, E., & Valdes-Sosa, P. A. (2018). Restate the reference for EEG microstate analysis. arXiv preprintarXiv:1802.02701.

Hu, W., Zhang, Z., Zhang, L., Huang, G., Li, L., & Liang, Z. (2022). Microstate detection in naturalistic electroencephalography data: A systematic comparison of topographical clustering strategies on an emotional database. *Frontiers in Neuroscience*, *16*, 812624.

Inouye, T., Shinosaki, K., Iyama, A., & Matsumoto, Y. (1993). Localization of activated areas and directional EEG patterns during mental arithmetic. *Electroencephalography and Clinical Neurophysiology*, *86*(4), 224–230.

Jerath, R., & Barnes, V. A. (2009). Augmentation of mind-body therapy and role of deep slow breathing. *Journal of Complementary and Integrative Medicine*, *6*(1).

Katayama, H., Gianotti, L. R., Isotani, T., Faber, P. L., Sasada, K., Kinoshita, T., & Lehmann, D. (2007). Classes of multichannel EEG microstates in light and deep hypnotic conditions. *Brain Topography*, *20*(1), 7–14.

Khanna, A., Pascual-Leone, A., & Farzan, F. (2014). Reliability of resting-state microstate features in electroencephalography. *PLoS One*, *9*(12), e114163.

Khanna, A., Pascual-Leone, A., Michel, C. M., & Farzan, F. (2015). Microstates in resting-state EEG: Current status and future directions. *Neuroscience & Biobehavioral Reviews*, *49*, 105–113.

Lehmann, D. (1990). Brain electric microstates and cognition: The atoms of thought. In *Machinery of the mind* (pp. 209–224). Springer.

Lehmann, D., Faber, P. L., Galderisi, S., Herrmann, W. M., Kinoshita, T., Koukkou, M., Mucci, A., Pascual-Marqui, R. D., Saito, N., Wackermann, J., Winterer, G., & Koenig, T. (2005). EEG microstate duration and syntax in acute, medicationnaive, first-episode schizophrenia: A multi-center study. *Psychiatry Research: Neuroimaging*, *138*(2), 141–156.

Lehmann, D., Ozaki, H., & Pal, I. (1987). EEG alpha map series: Brain microstates by space-oriented adaptive segmentation. *Electroencephalography and Clinical Neurophysiology*, *67*(3), 271–288.

Li, Y., Chen, G., Lv, J., Hou, L., Dong, Z., Wang, R., Su, M., & Yu, S. (2022). Abnormalities in resting-state EEG microstates are a vulnerability marker of migraine. *The Journal of Headache and Pain*, *23*(1), 1–12.

Lovallo, W. (1975). The cold pressor test and autonomic function: A review and integration. *Psychophysiology*, *12*(3), 268–282.

Michel, C. M., & Koenig, T. (2018). EEG microstates as a tool for studying the temporal dynamics of whole-brain neuronal networks: A review. *NeuroImage*, *180*, 577–593.

Mishra, A., Englitz, B., & Cohen, M. X. (2020). EEG microstates as a continuous phenomenon. *NeuroImage*, *208*, 116454.

Murray, M. M., Brunet, D., & Michel, C. M. (2008). Topographic ERP analyses: A step-by-step tutorial review. *Brain Topography*, *20*(4), 249–264.

Musso, F., Brinkmeyer, J., Mobascher, A., Warbrick, T., & Winterer, G. (2010). Spontaneous brain activity and EEG microstates. A novel EEG/FMRI analysis approach to explore resting-state networks. *NeuroImage*, *52*(4), 1149–1161.

Pan, J., & Tompkins, W. J. (1985). A real-time QRS detection algorithm. *IEEE Transactions on Biomedical Engineering*, *BME-32*(3), 230–236.

Park, H.-D., & Blanke, O. (2019). Heartbeat-evoked cortical responses: Underlying mechanisms, functional roles, and methodological considerations. *NeuroImage*, *197*, 502–511.

Pernice, R., Faes, L., Feucht, M., Benninger, F., Mangione, S., & Schiecke, K. (2022). Pairwise and higher-order measures of brain-heart interactions in children with temporal lobe epilepsy. *Journal of Neural Engineering*, *19*(4), 045002.

Pierpaolo, C., Franca, T., Gabriella, T., Patrique, F., Silvia, C., & Filippo, Z. (2022). Brain electrical microstate features as biomarkers of a stable motor output. *Journal of Neural Engineering*, *19*(5), 056042.

Pirondini, E., Coscia, M., Minguillon, J., Millan, J. D. R., van de Ville, D., & Micera, S. (2017). Eeg topographies provide subject-specific correlates of motor control. *Scientific Reports*, *7*(1), 1–16.

Pollatos, O., Kirsch, W., & Schandry, R. (2005). Brain structures involved in interoceptive awareness and cardioafferent signal processing: A dipole source localization study. *Human Brain Mapping*, *26*(1), 54–64.

Poulsen, A. T., Pedroni, A., Langer, N., & Hansen, L. K. (2018). Microstate EEGlab toolbox: An introductory guide. BioRxiv, 289850.

Quadt, L., Critchley, H., & Nagai, Y. (2022). Cognition, emotion, and the central autonomic network. *Autonomic Neuroscience*, *238*, 102948.

Rajendra Acharya, U., Paul Joseph, K., Kannathal, N., Lim, C. M., & Suri, J. S. (2006). Heart rate variability: A review. *Medical and Biological Engineering and Computing*, *44*(12), 1031–1051.

Schulz, S., Tupaika, N., Berger, S., Haueisen, J., Bar, K.-J., & Voss, A. (2013). Cardiovascular coupling analysis with high-resolution joint symbolic dynamics in patients suffering from acute schizophrenia. *Physiological Measurement*, *34*(8), 883–901.

Silvani, A., Calandra-Buonaura, G., Dampney, R. A., & Cortelli, P. (2016). Brain-heart interactions: Physiology and clinical implications. *Philosophical Transactions of the Royal Society A: Mathematical, Physical and Engineering Sciences*, *374*(2067), 20150181.

Skrandies, W. (1990). Global field power and topographic similarity. *Brain Topography*, *3*(1), 137–141.

Tait, L., Tamagnini, F., Stothart, G., Barvas, E., Monaldini, C., Frusciante, R., Volpini, M., Guttmann, S., Coulthard, E., Brown, J. T., Kazanina, N., & Goodfellow, M. (2020). EEG microstate complexity for aiding early diagnosis of alzheimer's disease. *Scientific Reports*, *10*(1), 1–10.

Tarvainen, M. P., Niskanen, J.-P., Lipponen, J. A., Ranta-Aho, P. O., & Karjalainen, P. A. (2014). Kubios HRV–heart rate variability analysis software. *Computer Methods and Programs in Biomedicine*, *113*(1), 210–220.

Thome, J., Densmore, M., Frewen, P. A., McKinnon, M. C., Theberge, J., Nicholson, A. A., Koenig, J., Thayer, J. F., & Lanius, R. A. (2017). Desynchronization of autonomic response and central autonomic network connectivity in posttraumatic stress disorder. *Human Brain Mapping*, *38*(1), 27–40.

Valenza, G., Citi, L., Saul, J. P., & Barbieri, R. (2018). Measures of sympathetic and parasympathetic autonomic outflow from heartbeat dynamics. *Journal of Applied Physiology*, *125*(1), 19–39.

Valenza, G., Passamonti, L., Duggento, A., Toschi, N., & Barbieri, R. (2020). Uncovering complex central autonomic networks at rest: A functional

magnetic resonance imaging study on complex cardiovascular oscillations. *Journal of the Royal Society Interface*, *17*(164), 20190878.

Valenza, G., Sclocco, R., Duggento, A., Passamonti, L., Napadow, V., Barbieri, R., & Toschi, N. (2019). The central autonomic network at rest: Uncovering functional mri correlates of time-varying autonomic outflow. *NeuroImage*, *197*, 383–390.

van de Ville, D., Britz, J., & Michel, C. M. (2010). EEG microstate sequences in healthy humans at rest reveal scale-free dynamics. *Proceedings of the National Academy of Sciences*, *107*(42), 18179–18184.

Wang, Q., & Sourina, O. (2013). Real-time mental arithmetic task recognition from EEG signals. *IEEE Transactions on Neural Systems and Rehabilitation Engineering*, *21*(2), 225–232.

Yao, D. (2001). A method to standardize a reference of scalp eeg recordings to a point at infinity. *Physiological Measurement*, *22*(4), 693–711.

Yu, X., Zhang, C., Su, L., Zhang, J., & Rao, N. (2018). Estimation of the cortico-cortical and brain-heart functional coupling with directed transfer function and corrected conditional entropy. *Biomedical Signal Processing and Control*, *43*, 110–116.

Yuan, H., Liu, T., Szarkowski, R., Rios, C., Ashe, J., & He, B. (2010). Negative covariation between task-related responses in alpha/beta-band activity and bold in human sensorimotor cortex: An eeg and fmri study of motor imagery and movements. *NeuroImage*, *49*(3), 2596–2606.

Zaccaro, A., Perrucci, M. G., Parrotta, E., Costantini, M., & Ferri, F. (2022). Brain-heart interactions are modulated across the respiratory cycle via interoceptive attention. *NeuroImage*, *262*, 119548.

Zappasodi, F., Croce, P., Giordani, A., Assenza, G., Giannantoni, N. M., Profice, P., Granata, G., Rossini, P. M., & Tecchio, F. (2017). Prognostic value of EEG microstates in acute stroke. *Brain Topography*, *30*, 698–710.

Zappasodi, F., Perrucci, M. G., Saggino, A., Croce, P., Mercuri, P., Romanelli, R., Colom, R., & Ebisch, S. J. (2019). EEG microstates distinguish between cognitive components of fluid reasoning. *NeuroImage*, *189*, 560–573.

Zygmunt, A., & Stanczyk, J. (2010). Methods of evaluation of autonomic nervous system function. *Archives of Medical Science*, *6*(1), 11–18.

Zyma, I., Tukaev, S., Seleznov, I., Kiyono, K., Popov, A., Chernykh, M., & Shpenkov, O. (2019). Electroencephalograms during mental arithmetic task performance. *Data*, *4*(1), 14.

SUPPORTING INFORMATION

Additional supporting information can be found online in the Supporting Information section at the end of this article.

How to cite this article: Catrambone, V., & Valenza, G. (2023). Microstates of the cortical brain-heart axis. *Human Brain Mapping*, 1–12. https://doi.org/10.1002/hbm.26480